

Article

Efficient Location and Extraction of the Iceberg Calved Areas of the Antarctic Ice Shelves

Mengzhen Qi ^{1,2,3} , Yan Liu ^{1,2,3}, Yijing Lin ^{1,3}, Fengming Hui ^{2,3,4}, Teng Li ^{1,2,3}
and Xiao Cheng ^{2,3,4,*}

¹ State Key Laboratory of Remote Sensing Science, and College of Global Change and Earth System Science, Beijing Normal University, Beijing 100875, China; 201921490035@mail.bnu.edu.cn (M.Q.); liuyan2013@bnu.edu.cn (Y.L.); 201921490033@mail.bnu.edu.cn (Y.L.); 201531490018@mail.bnu.edu.cn (T.L.)

² Southern Marine Science and Engineering Guangdong Laboratory, Zhuhai 519082, China; huifm@mail.sysu.edu.cn

³ University Corporation for Polar Research, Beijing 100875, China

⁴ School of Geospatial Engineering and Science, Sun Yat-Sen University, Zhuhai 519082, China

* Correspondence: chengxiao9@mail.sysu.edu.cn

Received: 14 July 2020; Accepted: 16 August 2020; Published: 18 August 2020



Abstract: Continuous, rapid, and precise monitoring of calving events contributes to an in-depth understanding of calving mechanisms, which have the potential to cause significant mass loss from the Antarctic ice sheet. The difficulties in the precise monitoring of iceberg calving lie with the coexistence of ice shelf advances and calving. The manual location of iceberg calving is time-consuming and painstaking, while achieving precise extraction has mostly relied on the surface textural characteristics of the ice shelves and the quality of the images. Here, we propose a new and efficient method of separating the expansion and calving processes of ice shelves. We visualized the extension process by simulating a new coastline, based on the ice velocity, and detected the calved area using the simulated coastline and single-temporal post-calving images. We extensively tested the validity of this method by extracting four annual calving datasets (from August 2015 to August 2019) from the Sentinel-1 synthetic aperture radar mosaic of the Antarctic coastline. A total of 2032 annual Antarctic calving events were detected, with areas ranging from 0.05 km² to 6141.0 km², occurring on almost every Antarctic ice shelf. The extraction accuracy of the calved area depends on the positioning accuracy of the simulated coastline and the spatial resolution of the images. The positioning error of the simulated coastline is less than one pixel, and the determined minimum valid extraction area is 0.05 km², when based on 75 m resolution images. Our method effectively avoids repetition and omission errors during the calved area extraction process. Furthermore, its efficiency is not affected by the surface textural characteristics of the calving fronts and the various changes in the frontal edge velocity, which makes it fully applicable to the rapid and accurate extraction of different calving types.

Keywords: Antarctica; ice shelves; iceberg calving; coastline; ice velocity; remote sensing

1. Introduction

The Antarctic ice shelf system is an important area connecting the ice sheets and the ocean. Its stability is closely related to the Antarctic mass balance. Iceberg calving, the shedding of ice from glaciers or ice shelf frontal edges, is the main process contributing to the dynamic mass loss from the ice sheet to the ocean. Iceberg calving accounts for half of the net mass loss of the Antarctic ice shelves [1–3]. Although iceberg calving plays an important role in the Antarctic ice shelf mass balance, the majority of the current ice sheet and ocean climate models do not represent the calving process in a physically realistic manner. Understanding this process is critical for accurately predicting the future impact of climate change on ice sheets.

Comprehensive and detailed observations of iceberg calving of different sizes help to accurately assess the mass loss and explore the calving mechanisms. The overall range of multiscale, large sample observations makes it possible to investigate this issue using statistical tools. For example, based on calving observations for Svalbard, Alaska, Greenland, and Antarctica, Åström et al. [4] found that calving events ranging from 1 m^3 to $1 \times 10^{12} \text{ m}^3$ follow a uniform statistical pattern. They revealed that the calving termini of the ice sheets and glaciers behave as self-organized critical systems. Medrzycka et al. [5] suggested the necessity of studying calving events of different magnitudes due to the variations in the physical mechanisms that triggered the phenomenon. Fine-scale monitoring of calving events is of great significance in improving the existing ice sheet models [6,7].

Currently, extensive and detailed iceberg calving observations are time-consuming and laborious. This is mainly because of the massive volume of high-resolution remotely sensed data and the lack of efficient extraction methods. This has led to a paucity of continuous monitoring of calving events at the continental scale. The most apparent manifestation of iceberg calving is the change in the coastline of the ice shelf's frontal edge. There are many methods to extract the coastline changes, before and after calving, which mainly fall into the following three categories: the manual extraction of coastlines in different phases [8,9], automatic extraction [10–12], and feature matching between different phase images to extract the advance and retreat of the coastline [13–15]. The first two methods measure the area changes of ice shelves as a whole, while the third one successfully separates the advance and retreat of the ice shelves from the total coastline change.

However, observing iceberg calving is much more complicated than monitoring changes in the coastline. This is because the expansion of the ice shelves coexists with the calving events, but the changes in the coastline can only reflect the overall advance or retreat of the coastline. One of the main objectives of the detailed monitoring of iceberg calving is to extract the location, shape, area, and mass of each single calving event. The National Ice Center (NIC) regularly releases iceberg locations throughout the year using multisource, high-resolution, remotely sensed data. This dataset is helpful to identify the locations of calving events, but the dataset includes only large icebergs. A number of large calving events are ice shelf collapses resulting from densely distributed rifts. A single collapse may produce numerous tiny icebergs, for example, the collapse and breaking up of the Larsen B Ice Shelf in March 2002 [16]. As for the extraction of a single calving event, Liu et al. [1] compiled a comprehensive inventory of annual Antarctic calving events larger than 1 km^2 from 2005 to 2011. They used a feature matching algorithm to match the images before and after calving events with the vectors of the ice shelf frontal edge and other distinct textural features. In some specific regions, they distinguished the calved area with the assistance of the GLAS (Geoscience Laser Altimeter System) elevation dataset and ice velocity. This is the first time that independent calving events have been separated from the overall advance–retreat of the coastline. However, this method requires repeated comparisons between the frontal edges in two temporal images to check whether calving has occurred, which is time-consuming and laborious. Moreover, the image matching method for high-precision monitoring is quite demanding in terms of the image's quality and texture coherence before and after calving.

In this study, we propose a new method of extracting the calved area. First, we developed a simulated coastline of another phase by adding the displacement, based on the ice velocity, to the position of the original coastline. Then, we compared the simulated coastline with the frontal edges in the corresponding remotely sensed images. Theoretically, the simulated coastline overlaps with the ice shelf's frontal edge where iceberg calving has not occurred. Thus, the calved area is the closure zone between the real and simulated coastlines. We validated the feasibility of this method by extracting the entire Antarctic calved area for four annual periods, from August 2015 to August 2019. Its advantages are as follows. In our method, calving events can be identified using single-phase images, in which the calved area is easy to distinguish. The extraction process has a high theoretical accuracy and strong adaptability, which also reduces the rate of repetition and omission in the detection. In addition, the differences in the frontal ice velocity and the image textural characteristics do not affect the extraction results.

2. Data

Satellite Imagery. The Sentinel-1 EW L1 ground range detected (GRD) products, which repeatedly covered the Antarctic coastline in August each year from 2015 to 2019, were used in our study. The data were downloaded from the European Space Agency (ESA) website (<https://www.esa.int/>). The Sentinel-1 constellation consists of two polar-orbiting satellites, each of which carries a dual-polarized C-band SAR (synthetic aperture radar) sensor with an operating frequency of 5.405 GHz. The revisit cycle of this binary system is about 6 days, but it can be shorter in higher latitudes. The extra-wide swath (EW) mode, which is one of the four operating modes, is mainly suitable for large, converging areas such as the polar regions. It has an imaging swath of 400 km and an orientation resolution of 40 m. The GRD products released by the core ground station record the signals of the backward scattering factor of the incident microwave radiation. They can perfectly reflect the geometry and electromagnetic properties of the objects being measured [17]. Therefore, we can distinguish between ice shelves and fast ice using the images, which is the basis for discovering calving events.

Grounding Line. The grounding line defines the extent of the ice shelves, setting it apart from the land ice. We used the MEaSURES (Making Earth System Data Records for Use in Research Environments) grounding line dataset version 2, downloaded from the National Snow and Ice Data Center (NSDIC) website (<https://nsidc.org/data/nsidc-0709/versions/2>). The MEaSURES project is one of the NASA's Earth Science Programs dedicating to advancing Earth remote sensing. This dataset was produced by extracting the grounding points from multiple satellites between 7 February 1992 and 31 December 2015. It provides comprehensive, high-resolution Antarctic grounding line datasets, with an accuracy of 25 m to 250 m, measured using D-InSAR (Differential Synthetic Aperture Radar Interferometry) technology [2,18,19].

Ice Velocity. We used the MEaSURES Antarctica Ice Velocity Map Version 2 to obtain the spatial distribution of the ice velocity values. It is a raster dataset with a 450 m × 450 m spatial resolution and a 20-year (1/1996–12/2016) temporal coverage that is extracted using Interferometric Synthetic Aperture Radar (InSAR). MEaSURES Antarctica Ice Velocity Map records the velocity value of each grid point in the X- and Y-directions with a well-corrected error of 17 m·a⁻¹. It can be downloaded from the NSDIC website (<https://nsidc.org/data/NSIDC-0484/versions/2>) [18,20,21].

3. Methods

Our methodology consisted of three parts: data preprocessing, iceberg calving extraction, and accuracy assessment. The data preprocessing included SAR image processing, ice velocity area extension, and benchmark ice shelf digitalization. The iceberg calving extraction included simulating the front edge of the different phases and detecting calving events from the simulated coastline and the corresponding images.

3.1. Data Preprocessing

SAR image processing. We processed the Sentinel-1 EW L1 GRD products using the Sentinel Application Platform (SNAP), developed by Brockmann Consult, SkyWatch and C-S and released by the the European Space Agency. After the calibration and terrain correction, we chose the Antarctica polar stereographic projections and resampled to a 75 m resolution. Then, we used ENVI (Environment for Visualizing Images), developed by Exelis Visual Information Solutions in the US, to mosaic the preprocessed images for each year, during which images with a date adjacent to 1 August would be put on the upper level to restrict the bias in imaging time. Figure 1 shows the SAR image processing results.

Ice velocity area extension. Glaciers are in constant motion. Therefore, the ice velocity product may not cover the newly advanced ice shelf's frontal edge. To solve this problem, we extended the area of the original raster dataset using the Moore-neighbor algorithm. Our methodology can be divided into three steps. First, identify the boundary between the empty and non-empty values of the ice velocity raster image. Next, assign values equal to the average of eight neighboring raster

cells to the empty center cells in a 3×3 window along the boundary. Then, iterate the first two steps 100 times to obtain the expanded ice velocity raster dataset. As for accuracy validation, the original ice velocity area was retreated inward by 2 km and then, it was iterated outward 50 times in the same way. We marked this result as a verification value. We calculated the average extension error by comparing the extended value to the verification value. The result shows that the error is about $8 \text{ m}\cdot\text{a}^{-1}$.

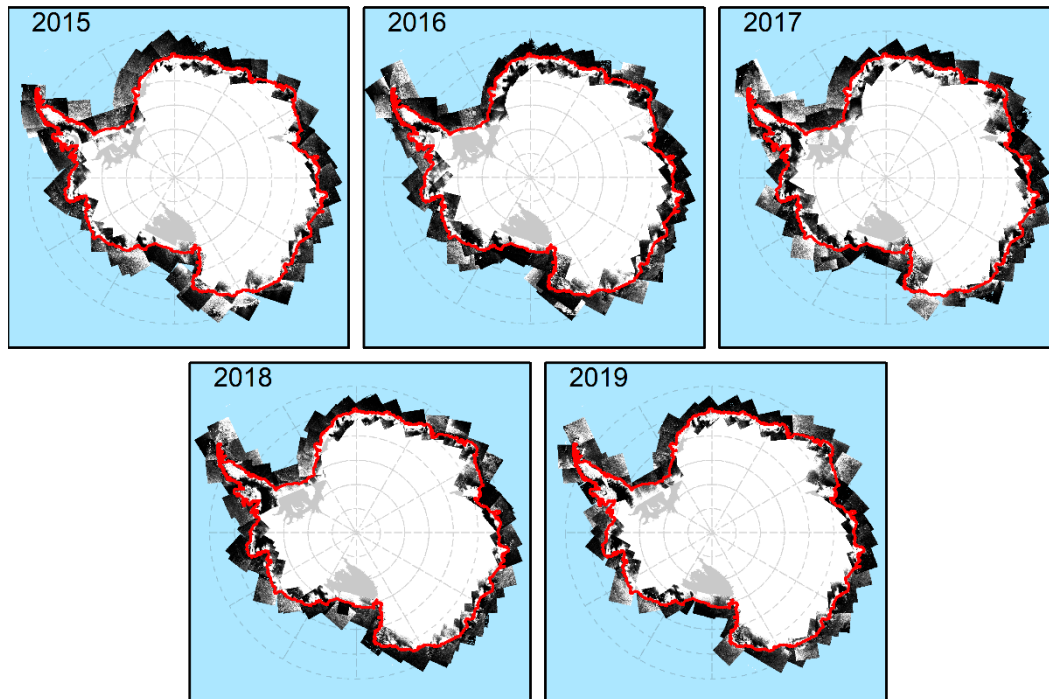


Figure 1. Annual Sentinel-1 synthetic aperture radar (SAR) mosaic of the Antarctic coastline in early August from 2015 to 2019.

Benchmark ice shelf digitalization. We automatically extracted and manually modified the coastline vector for August 2015 as the original coastline benchmark, using an updated version of the Canny edge detection algorithm. The accuracy was about 60 m [10]. Then, we checked the topological relationship between the grounding line vectors and the coastline vectors. To make sure the grounding line and the corresponding coastline were enclosed within closed polygons, we checked to make sure the coastline was continuous and each grounding line intersected with the coastline. We transformed the area enclosed by the ice shelf frontal coastlines and the grounding lines into polygons with a unique ID. Then, we obtained the accurate ice shelf outlines for August 2015, which were used as the input data for the following steps.

3.2. Iceberg Calving Extraction

Velocity-based ice shelf front edge simulation. We converted the benchmark ice shelf polygon vertices into points and recorded their order. Then, the following operations were carried out for each point. First, we judged whether the point was on the grounding line or not. Our study focused on the short-term front-edge changes, so we could assume no change had taken place in the position of the grounding line. Next, based on the velocity of each coastline point, we identified its movement and new location. After joining the points to the line, a new coastline was derived, namely the simulated coastline. The schematic of this process is shown in Figure 2.

Considering that the points in the fast flow regions may move more than one pixel in a month, we calculated the ice movement of each month and iterated for 12 times to obtain the annual ice movement, which means that the displacement of a coastline point in the fast flow region may be

determined by several different velocities, to improve the simulation accuracy. After traversing all of the points, we simulated the theoretical location of the coastline's feature points for the following year.

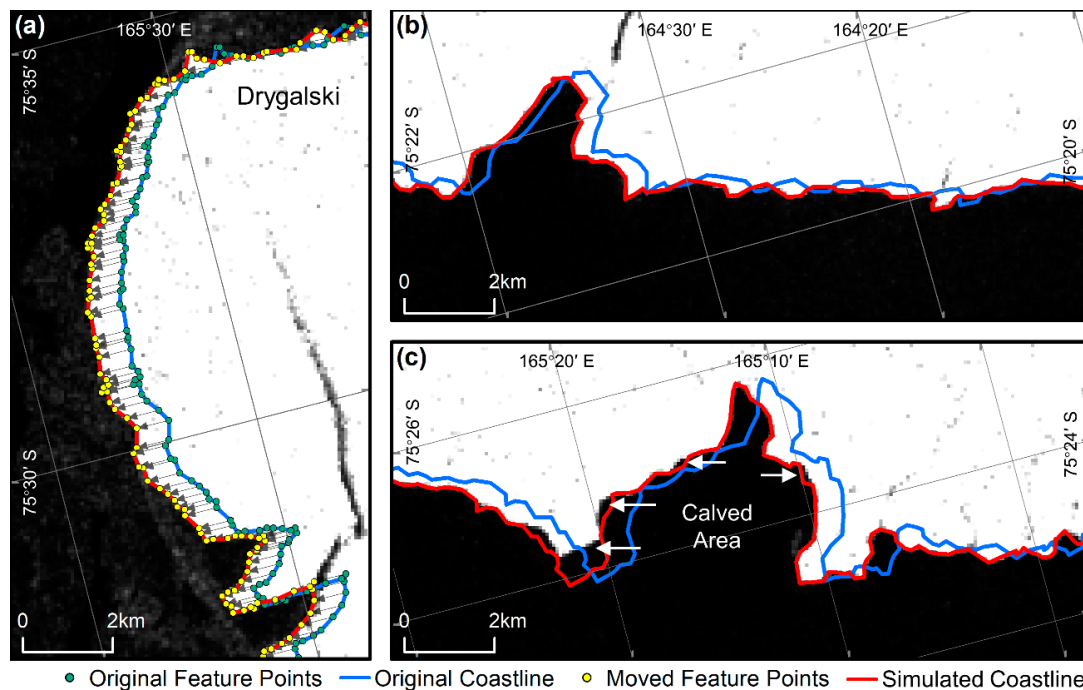


Figure 2. Schematic of the velocity-based ice shelf front-edge simulation. In panel (a), the blue line is the original coastline for the previous years, and the green points on the blue line are its feature points. The yellow points are the moving result of the green points based on the ice velocity. They represent the feature points of the next year's coastline. We connected the yellow points sequentially to generate the next year's simulated coastline (the red line). Panel (b) shows a no-calved scene. Panel (c) shows a calved scene, in which the calving events can be detected using the simulated coastline and the image.

Calved area extraction. An independent annual calving event is defined as its location not being spatially adjacent to other calving events in the same year. That is, all of the annual calving polygons during a specific year are not overlapped or adjacent in the projection space. The following year's simulated ice shelf polygons can be obtained by sequentially connecting the moved feature points with the grounding line points (the yellow line in Figure 3a). By comparing the simulated ice shelf polygon to its contemporaneous images and by correcting the frontal edge of the ice shelf, so that it fits into the actual coastline position, we can obtain the exact ice shelf polygon for the following year (the red line in Figure 3b). By subtracting the corrected ice shelf polygons from the theoretical simulated polygons, we obtained calved-area polygons during that year (blue translucent area in Figure 3c), meanwhile, we also obtained their shape and area properties under polar projection. By pushing the new, actual, coastline backward to the previous year's ice shelf, we found the fracture line and a similar blue translucent region overlap, between the polygon's outline and the fracture line (the black line in Figure 3d). We checked the topological relationships of all of the extracted regions in the same year for Antarctica, with the criterion that polygons do not intersect with each other. After the correction, we obtained vectors for each calved area during the year. While acquiring the calved areas, the coastlines were updated year by year. The updated coastlines can be regarded as benchmark coastlines for the next phase of the calving extraction.

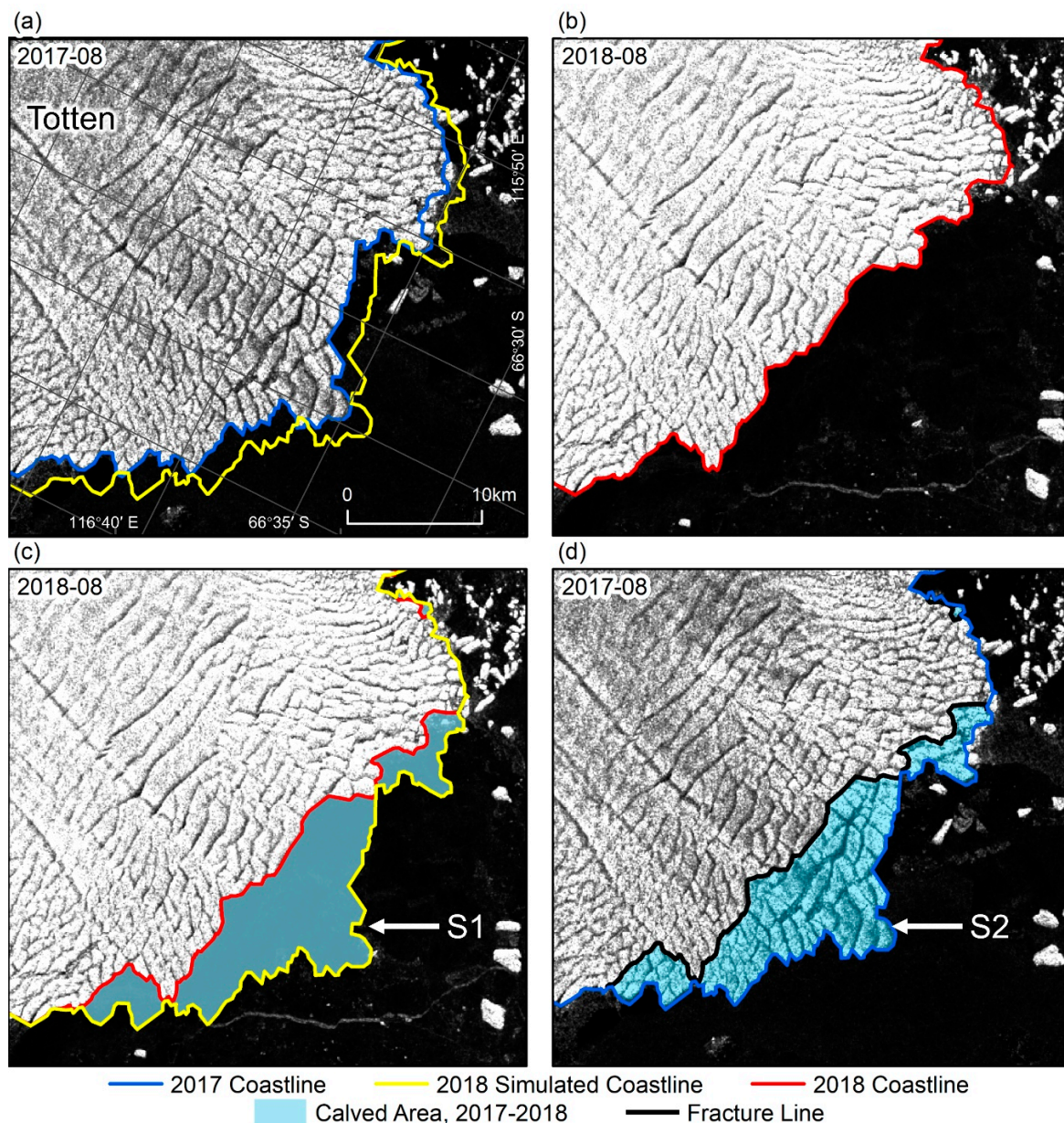


Figure 3. Schematic of the iceberg calving extraction. (a,d) displays the satellite images in August 2017, as well as (b,d) for images in August 2018. Blue lines in (a,d) represent the actual coastline in August 2017. Yellow lines in (a,c) indicate the simulated coastline in August 2018. Red lines in (b,c) stands for the actual coastline in August 2018. Blue area S1 shows the extraction result through our method, and S2 through the previous extraction method by feature tracking.

3.3. Accuracy Assessment

Positional accuracy of the simulated coastline. The samples from the ice shelves' frontal edges only advanced, but those without calving events were chosen to assess the accuracy of the simulated coastline. The specific method used is as follows. First, calculate the distance from the moved feature points on the simulated coastlines to the automatically extracted, and manually corrected, pixel boundaries of the ice shelves and the sea in the images. Then, determine the directions. If the feature points fall within the sea, the positional error is the distance value above. If the feature points fall on the ice shelf, the positional error is the negative value of the distance.

Extraction accuracy of the calved area. The samples of the calved areas with distinct fracture lines on the images were selected to assess the observation and extraction accuracy. For the calving

extraction from the same spatial resolution images, we compared the results obtained using our new method with those obtained using the previous method of image matching and feature tracking. The areas in our results (e.g., the blue translucent region in Figure 3c) are recorded as S1, and the areas in the control group (Figure 3d) are denoted as S2. We define S2 as the true value of the calved area and the difference between S1 and S2 (m^2) as the area extraction error. As the scale of each calving event varies, we use the error-equivalent perimeter width (m) to describe the accuracy. It is calculated by dividing the area extraction error by its perimeter.

Assessment of the minimum effective extraction area. We define the minimum effective extraction area as a value equal to the square of the product of the comprehensive error-equivalent pixel ($2\sqrt{2}$ times the ratio of the positional error to the spatial resolution of the images) and the image spatial resolution.

4. Results and Analysis

We randomly selected 30 sample boxes of $5\text{ km} \times 5\text{ km}$ (the locations are shown as red boxes in Figure 4) from the ice shelves' frontal edges where only advancement and no calving occurred to validate the positional accuracy of the simulated coastline. We also chose 30 calved-area samples (blue boxes in Figure 4) with distinct fracture lines to assess the extraction accuracy. Furthermore, we extensively tested the validity and efficiency of this method by extracting four interannual calving datasets from the Sentinel-1 SAR mosaic of the Antarctic coastline in August from 2015 to 2019.

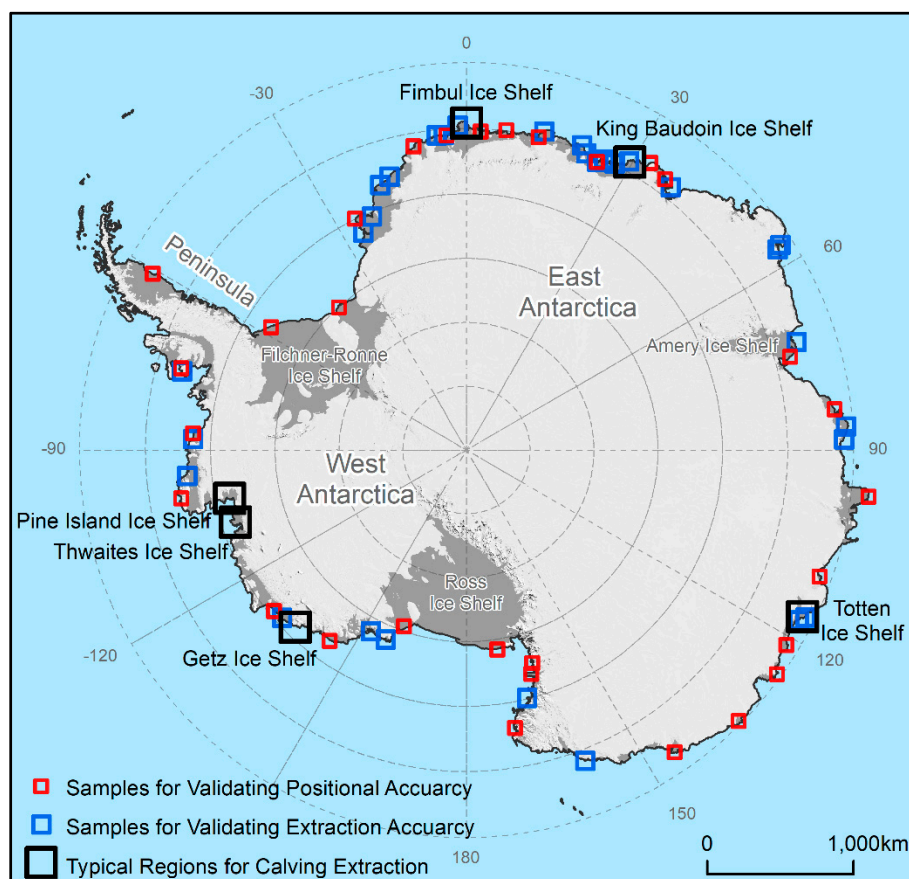


Figure 4. Spatial distribution of the samples and test areas overlain on the Moderate-resolution Imaging Spectroradiometer (MODIS) based Mosaic of Antarctica (MOA) (adapted from [22]). Red boxes show the samples used to verify the positional accuracy of the simulated coastlines, the blue boxes indicate the samples used to assess the extraction accuracy, and the black boxes represent the locations of six typical regions.

4.1. Positional Accuracy of the Simulated Coastline

The details of each sample are shown in Figure 5.

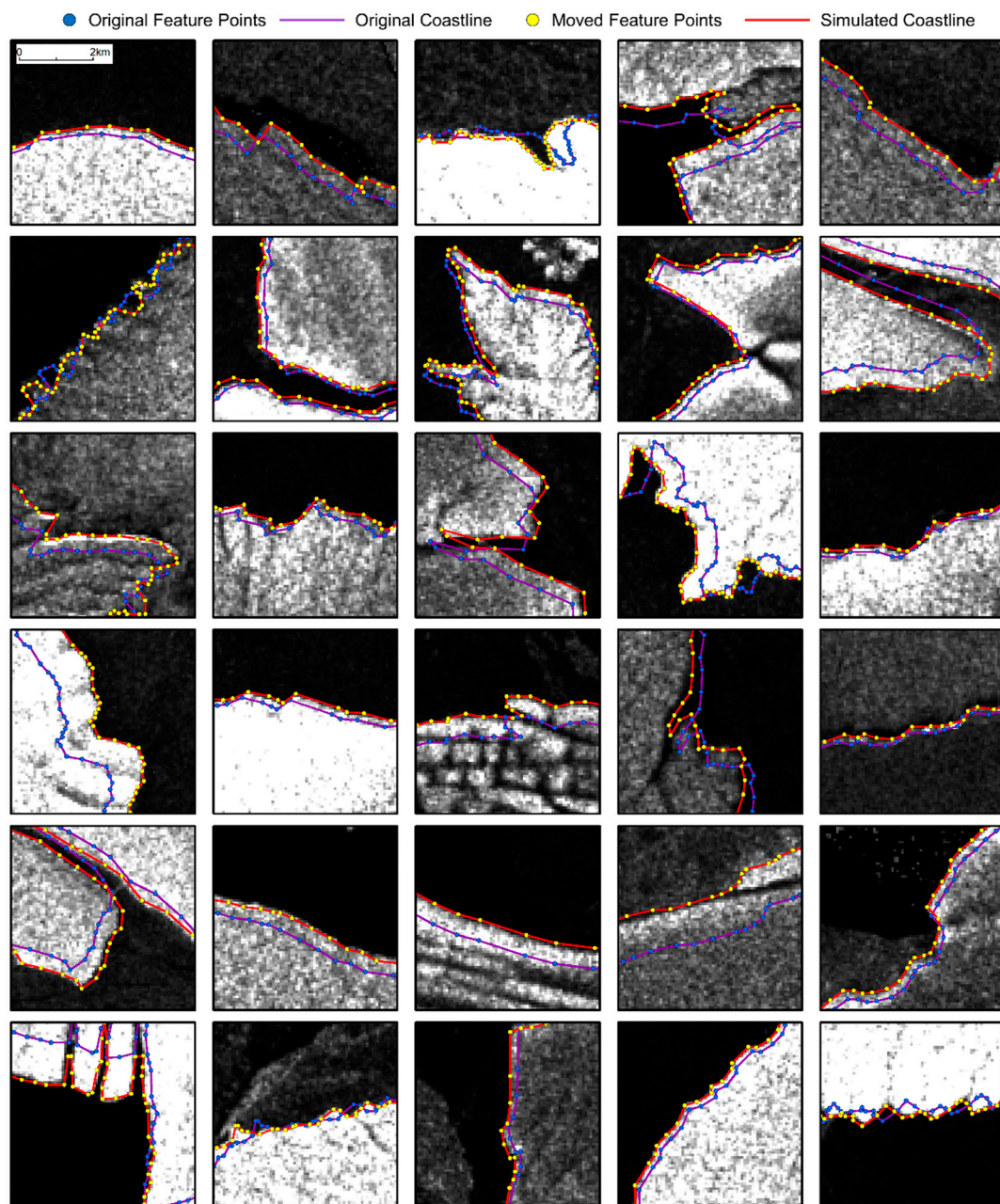


Figure 5. Samples used to validate the positional accuracy of the simulated coastline. The purple lines are the benchmark coastlines of the ice shelf’s frontal edge in 2015. The blue points and yellow points are feature points before and after moving based on the ice velocity, respectively. The red lines are the simulated coastlines in 2016 generated by sequentially connecting the yellow points. The sample locations are shown in Figure 4.

We measured the positional errors of all of the feature points (752 in total) in 30 samples. As is shown in Figure 6a, the errors generally exhibit a normal distribution with a standard deviation of 74.6 m and a mean value of 27.9 m. To some extent, there is a systematic error. This is because we regarded the distance from the feature points to the edge of the raster as the positional error, when in fact, the edge pixels are usually mixed pixels of ice and water.

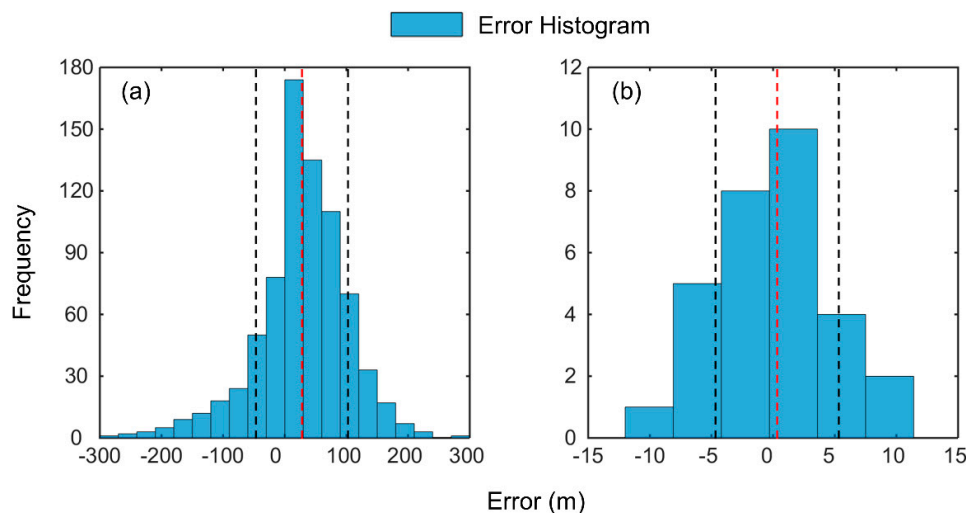


Figure 6. Error distribution histogram. The red and black vertical dashed lines represent the mean error and the standard deviation of error frequency distribution, respectively. (a) The positional error and (b) the extraction error in the form of error-equivalent perimeter widths.

4.2. Extraction Accuracy of the Calved Area

The extraction accuracy depends on the positional accuracy of the simulated coastline and the spatial resolution of the images. In 30 samples of calved areas, the error-equivalent perimeter widths of each calving event ranged from -9.2 m to 10.9 m, with a standard deviation of 5.0 m (Figure 6b). By synthesizing the accuracy analysis above, we conclude that based on the 75 m resolution SAR images, lengths greater than three pixels, both along and perpendicular to the ice flow direction, are valid. That is, the minimum effective extraction area in this study is about 0.05 km².

4.3. Extraction Results

In the time interval we studied, 2032 annual Antarctic calving events were detected with areas ranging from 0.05 km² to 6141.0 km² (Table 1). We found that as the calving scale decreases, its frequency increases exponentially, which means that the monitoring workload also increases exponentially. Among them, there were 1209 calving events smaller than 1 km², with a total area of 483.7 km² and an average annual area ratio of 4.1% . In particular, in 2017–2018, the total calved area of the smallest scale accounts for the highest proportion (8.9%), compared with the same scales in other years. Therefore, smaller-scale calving events cannot be ignored in the accurate estimation of mass loss, which highlights the importance of precisely monitoring iceberg calving.

Table 1. Statistics on iceberg calving at different scales from August 2015 to August 2019.

Year		<1 km ²	1–10 km ²	10–100 km ²	100–1000 km ²	>1000 km ²	Total
2015–2016	Frequency	322	162	34	9	1	528
	Area	134.0	515.4	1116.8	3058.3	893.9	5718.4
	Area ratio	2.3%	9.0%	19.5%	53.5%	15.6%	-
2016–2017	Frequency	210	167	50	6	1	434
	Area	91.2	563.0	1478.2	1077.9	6141.0	9351.4
	Area ratio	1.0%	6.0%	15.8%	11.5%	65.7%	-
2017–2018	Frequency	361	145	21	2	0	529
	Area	135.4	460.1	516.8	409.5	-	1521.7
	Area ratio	8.9%	30.2%	34.0%	26.9%	-	-
2018–2019	Frequency	316	198	22	5	0	541
	Area	123.1	610.1	478.3	1717.9	-	2929.5
	Area ratio	4.2%	20.8%	16.3%	58.6%	-	-

Figure 7 shows the spatial distribution of the different scale calving events. Tiny ($<1 \text{ km}^2$) and small scale ($1\text{--}10 \text{ km}^2$) calving events occurred on almost every Antarctic ice shelf. The former appeared most frequently in western Antarctica and the Queen Maud Land region in eastern Antarctica. The latter was common in western Antarctica, but in the Queen Maud Land region in eastern Antarctica, it occurred less often. Medium-scale ($10\text{--}100 \text{ km}^2$) calving events occurred frequently in eastern Antarctica between the Amery Ice Shelf and the Ross Ice Shelf, and in western Antarctica between the Ross Ice Shelf and the Antarctic Peninsula. Large-scale ($100\text{--}1000 \text{ km}^2$) and extra-large ($>1000 \text{ km}^2$) calving events occurred sporadically.

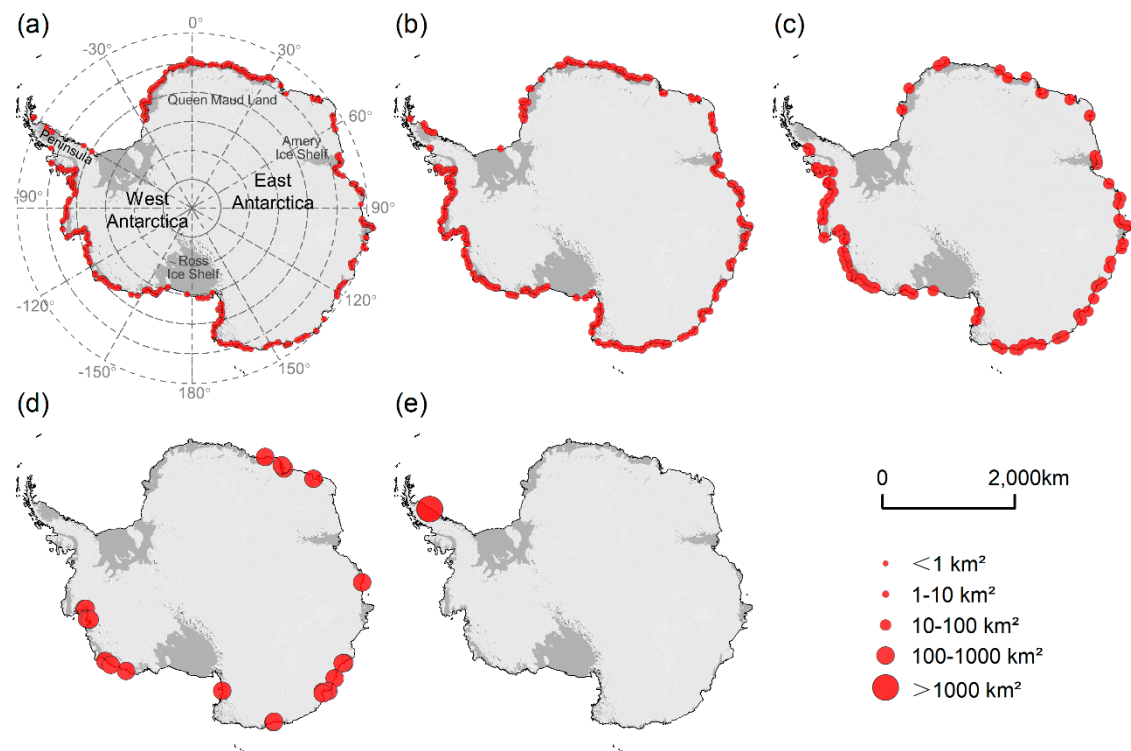


Figure 7. Spatial distribution of iceberg calving at different scales from August 2015 to August 2019. (a) Tiny-scaled ($<1 \text{ km}^2$); (b) Small-scaled ($1\text{--}10 \text{ km}^2$); (c) Medium-scaled ($10\text{--}100 \text{ km}^2$); (d) Large-scaled ($100\text{--}1000 \text{ km}^2$); (e) extra-large scaled ($>1000 \text{ km}^2$).

5. Discussion

As little research has been conducted on the precise extraction of independent calving events, some exploration has been done in our study to improve the extraction permanence at the full Antarctic scale. In this section, the accuracy, efficiency, and comparisons with traditional methods in typical regions are discussed.

The extraction accuracy depends on the spatial resolution of the images and the accuracy of the input coastline. Considering that August is the Austral winter, during which the calving frequency is lower than in other months [4], we used early August from one year to the next year as the extraction cycle. For the image time selection, priority was given to images from early August, and the missing parts were filled in with other nearby times. To some extent, this operation can miss the occurrence of calving events within the tiny time interval covered by the images, which may cause the misjudgment of the year. In terms of the imagery source selection, August is the polar night in Antarctica, during which optical sensors do not work well; therefore, SAR images covering the Antarctic coastline with a shorter revisit period were selected. As for the input coastline, we chose one for which both the accuracy and the temporal coverage fit our needs from a number of Antarctic coastline products. We also performed some manual corrections to make it more applicable as an input for this method.

In terms of the extraction efficiency, combined with the simulated coastline, this method can detect different types of calving using only single-phase images of the post-calving coastline, which greatly expedites the extraction process. We determined that in only 3–5 h, we can obtain the overall calving events for the Antarctic ice shelves in one year based on 75 m resolution image data.

Then, we further illustrated the advantages of our method using six typical regions (black boxes in Figure 4) with different calving characteristics as examples.

5.1. Detection of Infrequent Tabular Calving Events

Infrequent tabular calving is mostly dominated by stresses propagating along preexisting crevasses, and it has longer recurrence intervals in the same spatial neighborhood [1]. We can see the obvious fracture line and only one or two tabular icebergs in the pre-calving and post-calving images.

The Ross, Ronne-Filchner, and Amery ice shelves, the Larsen C Ice Shelf on the Antarctic Peninsula, and the large ice shelves in the Queen Maud Land region are relatively stable overall, with slow ice velocities. The expansion of rifts on the surface triggers fracturing and calving.

For example, in the test areas on the Fimbul Ice Shelf and the King Baudoin Ice Shelf, significant rift-opening disintegration only occurred in 2015–2016 (Figure 8). The shape and location of the calved areas are visible on the pre- and post-disintegration images. The occurrence of such infrequent and crevasse-distinct iceberg calving events can be accurately monitored using both our proposed method and previous methods [1].

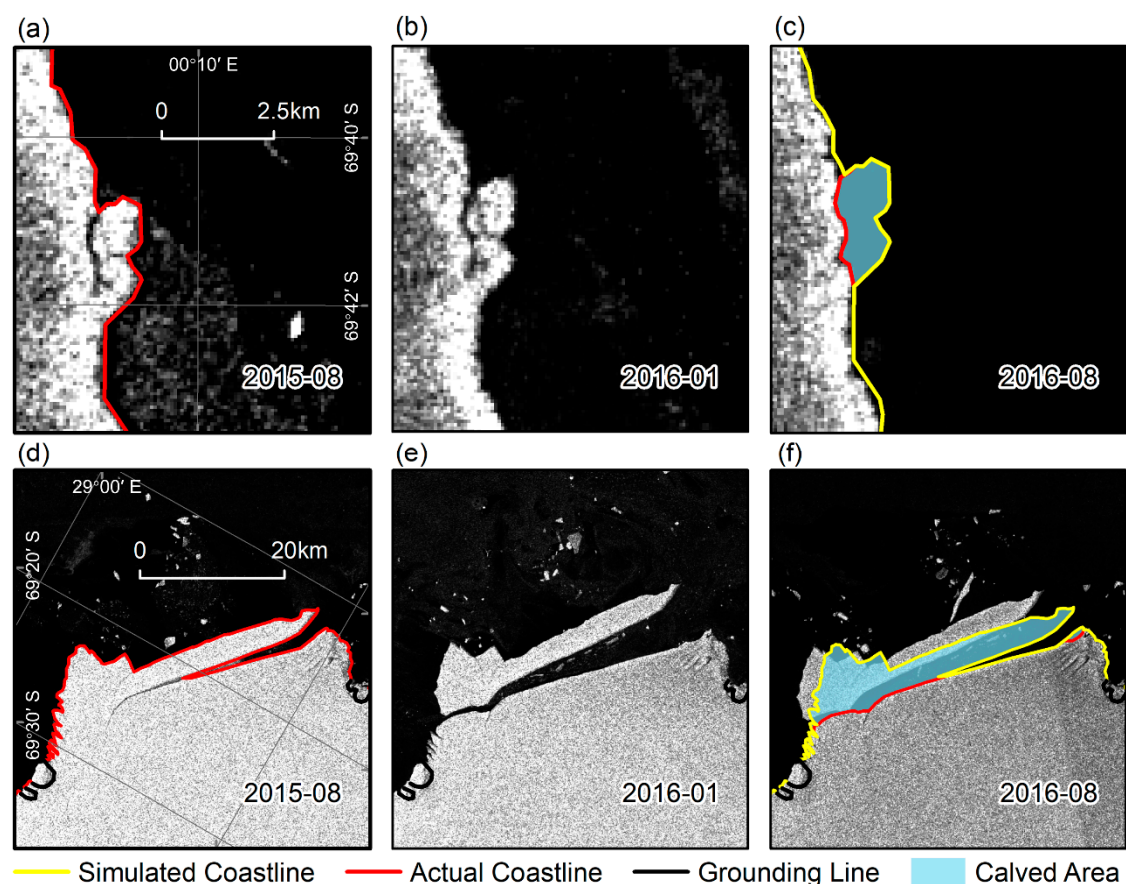


Figure 8. Extraction results of the infrequent “tabular” calving. (a–c) for test area in the Fimbul ice shelf, and (d–f) for the King Baudoin ice shelf, respectively. Locations are shown in Figure 4.

5.2. Detection of Frequent Disintegration Calving Events

Frequent disintegration calving is mainly associated with the basal and/or surface melting of ice shelves, and it has shorter recurrence intervals in the same spatial neighborhood [2]. Most of the

pre-disintegration images have a high density of crevasses. After disintegration, numerous small, fragmented icebergs are present. These icebergs remain drifting near the calving front for some time, which causes difficulties for traditional calved-area extraction by image matching. Our coastline simulation monitoring method is not subject to the textural characteristics of the images before and after the disintegration. Therefore, it is more advantageous for extracting this type of iceberg calving. Figure 9 shows the extraction results for four consecutive years within the test areas.

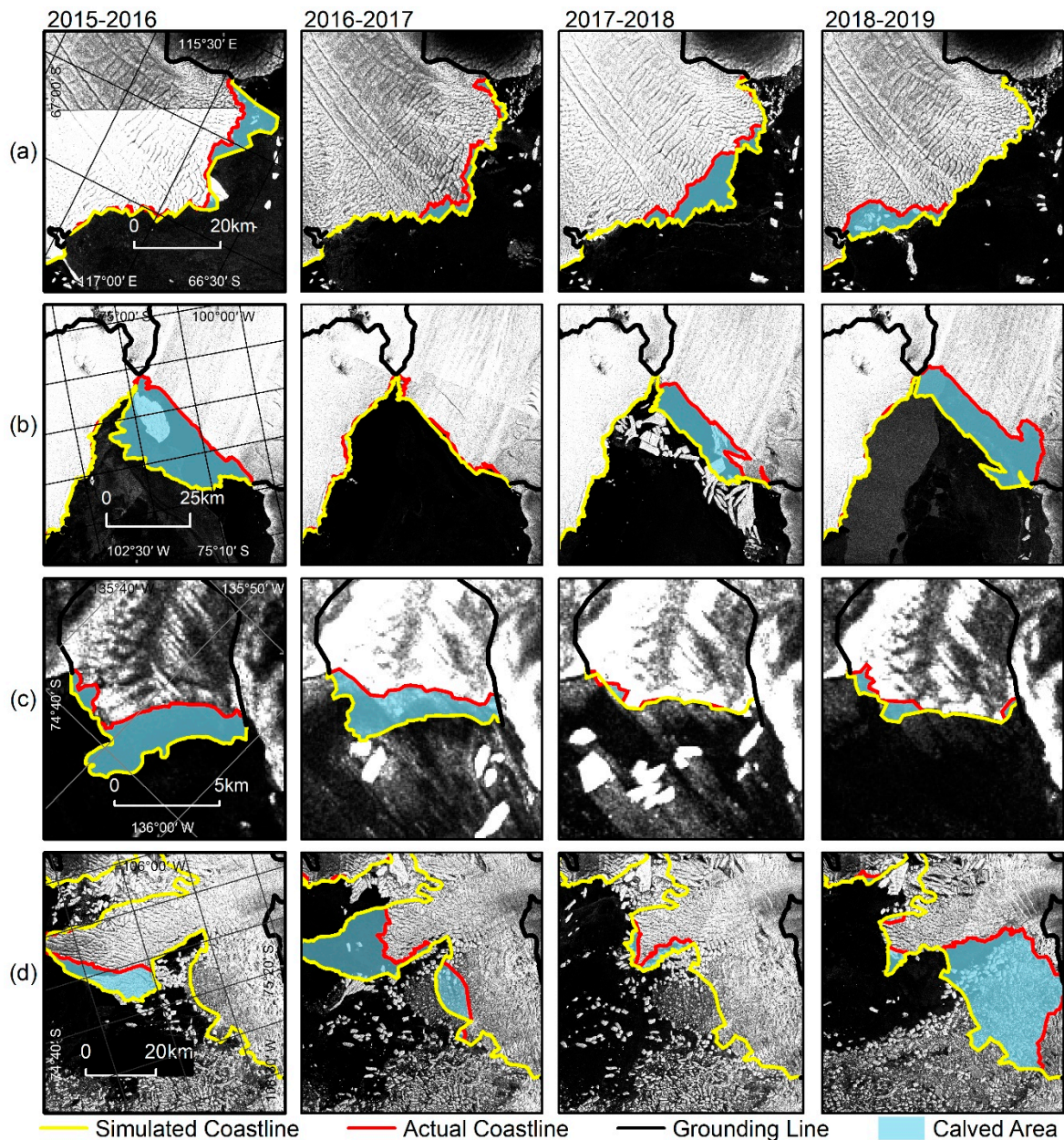


Figure 9. Extraction results of the frequent “disintegration” calving. Test area located in (a) the Totten ice shelf; (b) the Pine Island ice shelf; (c) the Getz ice shelf, and (d) the Thwaites ice shelf. Locations are shown in Figure 4.

The frontal edge of the Totten Ice Shelf is in rapid advance–retreat. During 2015–2019, calving events occurred sequentially at various locations along its coastline in a clockwise direction in the test area (Figure 9a). Although fracture lines are evident in the images before and after the disintegration, the large difference in the velocity direction at the frontal edge causes errors in the feature tracking.

In contrast, our method incorporates the velocity variables into the frontal edge simulation, so the detection results are not affected by the differences in the frontal ice velocities.

The frontal edge of the Pine Island Ice Shelf is also in rapid advance–retreat. Large disintegrations ($>100\text{ km}^2$) occurred in this test area during 2015–2016, 2017–2018, and 2018–2019. However, in 2016–2017, we extracted only six small disintegrations of $<15\text{ km}^2$ (Figure 9b). This demonstrates that small, sporadic calving that occurs after large disintegrations can be detected using our proposed method.

The test area on the Getz Ice Shelf is the smallest (i.e., only $1\text{ km} \times 1\text{ km}$). The total areas of disintegration during 2015–2019 were 114.7 km^2 , 11.4 km^2 , 0.7 km^2 , and 2.5 km^2 (Figure 9c). Such small-scale iceberg calving events are often missed. Furthermore, there are no obvious textures in the images, which makes it impossible to detect the calved areas through feature tracking. Using our method, the disintegration region can be finely extracted, regardless of the image texture characteristics.

The Thwaites Ice Shelf is fast-flowing, with typical frequent disintegration calving events occurring in each of the four years (Figure 9d). Numerous crevasses and fragmented icebergs characterize the images of these calving areas, but detection using a simulated coastline and a single post-calving image is still applicable and accurate.

6. Conclusions

The difficulties in the precise monitoring of individual calving events lie in the coexistence of advance and retreat of the ice shelf's frontal edge. Calved areas cannot be directly captured by only detecting changes in the coastlines. Traditional extraction methods, which can be time-consuming and laborious, rely heavily on the textural characteristics and the quality of the images. To deal with these difficulties and deficiencies, we developed a new method using the ice velocity and remotely sensed imagery for the rapid, accurate, and precise extraction of iceberg calving.

We separated the changes in the ice shelf's frontal edge into two processes: expansion and calving. The expansion can be visualized as a simulated coastline created by adding the ice velocity to the pre-calving coastline. Then, we detected the calved area using the simulated coastline and the post-calving images. While acquiring the calved areas, the coastlines were updated year by year. The updated coastlines can be regarded as benchmark coastlines for the next phase of the calving extraction. This effectively avoids omission and repetition errors in a long sequence. The accuracy of this method depends on the ice velocity error and the spatial resolution of the images. Using the latest ice velocity data and 75 m resolution images, the positional accuracy of the simulated coastlines is $\pm 74.6\text{ m}$, which is less than one pixel. As both the positional error and the manual extraction error are not systematic biased, the extraction accuracy is equivalent to only 5.0 m on the perimeter, which is almost negligible. Based on the positioning accuracy, we conclude that the minimum effective extraction area of iceberg calving based on 75 m resolution SAR data is 0.05 km^2 .

We extensively tested the validity and efficiency of our proposed method by extracting annual calving events at each scale between August 2015 and August 2019, using the Sentinel-1 SAR mosaic of the Antarctic coastline. Compared with the method of Liu et al. [1], the simulation of the advance of the ice shelves' frontal edge effectively avoids the omission of small calving events, caused by repeatedly comparing the changes in two temporal-phase images. It also saves a lot of time. In addition, we can accurately acquire the calved areas by comparing only the simulated ice shelf's frontal edge with the post-calving edge in the images, which avoids the time-consuming extraction task of matching features from dual images and relieves the requirement for image quality and textural features. In the four-year interval we studied, 2032 annual calving events were detected in Antarctica, of which 1209 were smaller than 1 km^2 , with a total area of 483.7 km^2 and a maximum annual area ratio of 8.9%. Therefore, small-scale calving events cannot be ignored in the accurate estimation of mass loss, and the precise monitoring of iceberg calving is meaningful. Furthermore, we determined the extraction effect of six typical test areas with different calving characteristics. The results demonstrate that this new method can effectively achieve iceberg calving extraction in various situations, including but not

limited to, areas with numerous crevasses, broken iceberg patches, widely varying frontal ice velocities, and little apparent surface texture.

In conclusion, this calving extraction method has a simple implementation, a wide applicability, a fine extraction accuracy, and a high efficiency. This method has been automated for coastline extension based on ice velocity. The manual extraction process can be automated in the future. Nevertheless, the manual extraction efficiency of this method is already very high, unless the automatic extraction is sufficiently accurate to eliminate the post-processing process of visual inspection, it may not have a superior efficiency. The idea of separating the advance and retreat of ice shelves, used in this method, can be used for the automatic extraction of coastlines in long time series. Compared with the traditional automatic coastline extraction method, the manual post-processing of coastline splicing is eliminated, and the interference of the automatically identified sea ice in the optical images is effectively reduced. We are now using this method to complete the precise extraction of a longer sequence of iceberg calving inventory.

Author Contributions: Conceptualization, Y.L. (Yan Liu) and M.Q.; methodology, Y.L. (Yan Liu), M.Q. and Y.L. (Yijing Lin); validation, M.Q.; formal analysis, M.Q.; data curation, Y.L. (Yan Liu) and M.Q.; writing—original draft preparation, M.Q.; writing—review and editing, Y.L. (Yan Liu), X.C., F.H. and T.L.; visualization, M.Q.; supervision, Y.L. (Yan Liu), X.C.; project administration, X.C.; funding acquisition, X.C. All authors have read and agreed to the published version of the manuscript.

Funding: This research was funded by the National key research and development Program of China (Grant No. 2018YFA0605403), National Natural Science Foundation of China (Grant No. 41925027), and Qian Xuesen Lab.—DFH Sat. Co. Joint Research and Development Fund.

Acknowledgments: We greatly thank ESA for providing the Sentinel-1A (<https://www.esa.int/>) imagery, and we truly appreciate the National Snow and Ice Data Center (<https://nsidc.org/data>) for providing the ice velocity and grounding line products.

Conflicts of Interest: The authors declare no conflict of interest.

References

1. Liu, Y.; Moore, J.C.; Cheng, X.; Gladstone, R.M.; Bassis, J.N.; Liu, H.; Wen, J.; Hui, F. Ocean-driven thinning enhances iceberg calving and retreat of Antarctic ice shelves. *Proc. Natl. Acad. Sci. USA* **2015**, *112*, 3263–3268. [[CrossRef](#)] [[PubMed](#)]
2. Rignot, E.; Jacobs, S.; Mouginot, J.; Scheuchl, B. Ice-shelf melting around Antarctica. *Science* **2013**, *341*, 266–270. [[CrossRef](#)] [[PubMed](#)]
3. Depoorter, M.A.; Bamber, J.L.; Griggs, J.A.; Lenaerts, J.T.; Ligtenberg, S.R.; van den Broeke, M.R.; Moholdt, G. Calving fluxes and basal melt rates of Antarctic ice shelves. *Nature* **2013**, *502*, 89–92. [[CrossRef](#)] [[PubMed](#)]
4. Åström, J.A.; Vallot, D.; Schäfer, M.; Welty, E.Z.; O’Neel, S.; Bartholomäus, T.C.; Liu, Y.; Riikilä, T.I.; Zwinger, T.; Timonen, J.; et al. Termini of calving glaciers as self-organized critical systems. *Nat. Geosci.* **2014**, *7*, 874–878. [[CrossRef](#)]
5. Medrzycka, D.; Benn, D.I.; Box, J.E.; Copland, L.; Balog, J. Calving Behavior at Rink Isbrae, West Greenland, from Time-Lapse Photos. *Arct. Antarct. Alp. Res.* **2016**, *48*, 263–277. [[CrossRef](#)]
6. Pattyn, F.; Morlighem, M. The uncertain future of the Antarctic Ice Sheet. *Science* **2020**, *367*, 1331–1335. [[CrossRef](#)]
7. Massom, R.A.; Scambos, T.A.; Bennetts, L.G.; Reid, P.; Squire, V.A.; Stammerjohn, S.E. Antarctic ice shelf disintegration triggered by sea ice loss and ocean swell. *Nature* **2018**, *558*, 383–389. [[CrossRef](#)]
8. Moon, T.; Joughin, I. Changes in ice front position on Greenland’s outlet glaciers from 1992 to 2007. *J. Geophys. Res.* **2008**, *113*. [[CrossRef](#)]
9. Murray, T.; Scharrer, K.; Selmes, N.; Booth, A.D.; James, T.D.; Bevan, S.L.; Bradley, J.; Cook, S.; Llana, L.C.; Drocourt, Y.; et al. Extensive retreat of Greenland tidewater glaciers, 2000–2010. *Arct. Antarct. Alp. Res.* **2015**, *47*, 427–447. [[CrossRef](#)]
10. Yu, Y.; Zhang, Z.; Shokr, M.; Hui, F.; Cheng, X.; Chi, Z.; Heil, P.; Chen, Z. Automatically Extracted Antarctic Coastline Using Remotely-Sensed Data: An Update. *Remote Sens.* **2019**, *11*, 1844. [[CrossRef](#)]

11. Seale, A.; Christoffersen, P.; Mugford, R.I.; O'Leary, M. Ocean forcing of the Greenland Ice Sheet: Calving fronts and patterns of retreat identified by automatic satellite monitoring of eastern outlet glaciers. *J. Geophys. Res.* **2011**, *116*. [[CrossRef](#)]
12. Mohajerani, Y.; Wood, M.; Velicogna, I.; Rignot, E. Detection of Glacier Calving Margins with Convolutional Neural Networks: A Case Study. *Remote Sens.* **2019**, *11*, 74. [[CrossRef](#)]
13. Cook, A.J.; Fox, A.J.; Vaughan, D.G.; Ferrigno, J.G. Retreating glacier fronts on the Antarctic Peninsula over the past half-century. *Science* **2005**, *308*, 541–544. [[CrossRef](#)] [[PubMed](#)]
14. Cook, A.J.; Vaughan, D.G. Overview of areal changes of the ice shelves on the Antarctic Peninsula over the past 50 years. *Cryosphere* **2010**, *4*, 77–98. [[CrossRef](#)]
15. Xin, Z.; Chun-Xia, Z.; Dong-Chen, E.; Jia-Chun, A. Monitoring the change of Antarctic ice shelves and coastline based on multiple-source remote sensing data. *Chin. J. Geophys.* **2013**, *56*, 3302–3312. [[CrossRef](#)]
16. Scambos, T.; Hulbe, C.; Fahnestock, M. Climate-Induced Ice Shelf Disintegration in the Antarctic Peninsula. In *Antarctic Peninsula Climate Variability: Historical and Paleoenvironmental Perspectives*; The American Geophysical Union: Washington, DC, USA, 2003; pp. 79–92. [[CrossRef](#)]
17. Koppel, K.; Zalite, K.; Voormansik, K.; Jagdhuber, T. Sensitivity of Sentinel-1 backscatter to characteristics of buildings. *Int. J. Remote Sens.* **2017**, *38*, 6298–6318. [[CrossRef](#)]
18. Rignot, E.; Mouginot, J.; Scheuchl, B. Ice flow of the Antarctic ice sheet. *Science* **2011**, *333*, 1427–1430. [[CrossRef](#)]
19. Rignot, E.; Mouginot, J.; Morlighem, M.; Seroussi, H.; Scheuchl, B. Widespread, rapid grounding line retreat of Pine Island, Thwaites, Smith, and Kohler glaciers, West Antarctica, from 1992 to 2011. *Geophys. Res. Lett.* **2014**, *41*, 3502–3509. [[CrossRef](#)]
20. Mouginot, J.; Scheuchl, B.; Rignot, E. Mapping of Ice Motion in Antarctica Using Synthetic-Aperture Radar Data. *Remote Sens.* **2012**, *4*, 2753–2767. [[CrossRef](#)]
21. Mouginot, J.; Rignot, E.; Scheuchl, B.; Millan, R. Comprehensive Annual Ice Sheet Velocity Mapping Using Landsat-8, Sentinel-1, and RADARSAT-2 Data. *Remote Sens.* **2017**, *9*, 364. [[CrossRef](#)]
22. Scambos, T.A.; Haran, T.; Fahnestock, M.; Painter, T.H.; Bohlander, J. MODIS-based Mosaic of Antarctica (MOA) data sets: Continent-wide surface morphology and snow grain size. *Remote Sens. Environ.* **2007**, *111*, 242–257. [[CrossRef](#)]



© 2020 by the authors. Licensee MDPI, Basel, Switzerland. This article is an open access article distributed under the terms and conditions of the Creative Commons Attribution (CC BY) license (<http://creativecommons.org/licenses/by/4.0/>).